

Event-driven simulation of a simple model for dense suspension flow

Edan Lerner¹, Gustavo Düring¹, and Matthieu Wyart¹

¹*Center for Soft Matter Research, Physics Department,
New York University, 4 Washington Place, New York, NY 10003*

Abstract

We introduce an event-driven simulation scheme for a simplified model of dense suspensions under flow. In this model, hydrodynamic interactions are neglected. The viscous drag force exerted on a particle is proportional to the difference between the fixed velocity of the underlying fluid, and the velocity of the particle. Our event-driven approach is based on an exactly-derivable equation of motion which depends solely on geometric information. Our method allows for a robust extraction of the instantaneous coordination of the particles as well as contact-forces statistics and dynamics, under any chosen mode of deformation. It can also be used for generating jammed packings under shear or compression.

1. Introduction

The viscosity of a suspension of immersed hard particles was computed early on by Einstein at low volume fraction ϕ [1]. At larger volume fractions ϕ , approaching random close packing ϕ_c where jamming occurs [2, 3], the viscosity diverges and the motion of the particles becomes increasingly correlated [4, 5]. These observations suggest that dense flows may be governed by a dynamical critical point. Understanding this critical behavior would resolve a geometrical question fundamental to various problems of condensed matter: how can particles move while still avoiding each other at high density?

Computer simulations are playing an increasingly important role in the investigation of the relationship between microscopic structure and rheology of amorphous systems – concentrated suspensions in particular – and are well suited to investigate this question. There exist a number of simulational methods for suspensions which take into account hydrodynamic, interparticle and Brownian interactions. These methods are reviewed in [4, 6]. In this work we study a model of suspensions where hydrodynamic interactions are neglected, which simplifies the dynamics considerably. This class of models has received a lot of attention recently [7, 8, 9, 10, 11, 12, 13, 14, 15] as they appear to capture, qualitatively at least, the observed presence of a jamming transition where the viscosity diverges.

The model under focus consists of rigid frictionless particles immersed in a flowing Newtonian fluid. The flow of the fluid is characterized by an affine velocity field, and the dynamics is assumed to be overdamped. Hydrodynamic interactions are neglected, such that the viscous drag forces acting on the particles are proportional to the difference between the particle velocities and the velocity of the underlying flowing fluid.

A similar model was initially proposed by Durian [9, 10] for the description of sheared foams, where soft repulsive interactions are introduced between the constituent bubbles. At packing fractions below jamming, the quasi-static limit (i.e. vanishing strain rate) of such a model corresponds to rigid-particle dynamics, as the soft particles always have enough time to rearrange to a state of vanishing energy, so that particles do not overlap. The quasi-static limit of this model was recently studied numerically by imposing vanishingly small stresses [7] or strain rates [8, 11, 12, 13]. Two methods have been employed to simulate this system: (i) small imposed strain increments are followed by the minimization of the potential energy [12, 13], or (ii) integration of the overdamped equations of motion, where the damping is proportional to the difference between the particles' velocities and the affine flow [7, 8, 11].

One difficulty of method (i) is that the energy landscape of soft particles below jamming displays many flat directions – the so-called floppy modes. Various minimization methods in quasi-static simulations may result in uncontrolled evolution along these floppy modes. The steepest descent minimization method does not face this problem, as in principle no undesired motion occurs along floppy modes during minimization. However, the usefulness of the steepest descent method is hampered by its extremely long running time in the quasi static limit. The integration of the overdamped equations of motion [8, 11] of method (ii) above requires ever-smaller strain rates to allow for enough time for the system to reorganize and relax towards the zero-energy states, in order to probe correctly the rigid particle limit. In practice the integration step is chosen to be rather large, allowing to probe large systems at the expense of loosing accuracy in the microscopic dynamics. Here we introduce a new method that allows us to extract precisely which contacts are present, how contacts appear and disappear, and how these events affect the contact forces throughout the sample. Our method also enforces the correct motion in the space of floppy modes, as steepest descent does, but it is less expensive computationally.

Our approach is based on the exactly derivable equations of motion in the hard sphere limit. These equations are used to build an event-driven simulation. The equations of motion are entirely based on geometric information, which allows for the calculation of contact forces between the constituent hard particles, and hence their distribution and evolution. The main idea is to evolve the system according to the equation of motion, while carefully handling the formation of new contacts and the opening of existing contacts between particles. Our method shares some similarities with the method of contact dynamics [16] used in dry granular materials, in which contact forces and velocities are resolved iteratively under a set of complementarity relations.

This paper is organized as follows: Sect. 2 describes the simplified model which our simulation

method follows. Sect. 3 derives the equation of motion for the presented model, building on its main assumptions. Sect. 4 illustrates the concept of the instantaneous contact network, which is geometric information on which the equation of motion is based. Sect. 5 contains an elaborate description of our simulational scheme and ends with a perscription for generating jammed configurations under shear or compression. Sect. 6 presents results from our simulations, illustrating the utility of our event driven approach. Sect. 7 presents concluding remarks.

2. Model of the flow of hard particles immersed in a viscous fluid

Consider a system of rigid frictionless spherical particles immersed in a viscous fluid, at a volume fraction ϕ . The fluid phase is assumed to flow with some affine velocity field denoted as \vec{V}^{fl} , and the particles are assumed not to alter the flow of the fluid phase. The fluid viscosity is η_0 , and the Reynold number is negligibly small.

These assumptions lead to two consequences:

- (i) The fluid exerts drag forces on the particles that are proportional to the difference between the particles' velocity and the velocity of the fluid at the position of the particles. Denoting the k^{th} particle's velocity by \vec{V}_k and its position by \vec{R}_k , the force exerted on this particle by the fluid is (see Fig. 1)

$$\vec{F}_k = -\eta_0 \left[\vec{V}_k - \vec{V}^{\text{fl}}(\vec{R}_k) \right] . \quad (1)$$

- (ii) The dynamics is overdamped, therefore forces on each particle are always balanced. Thus, the drag force exerted on the k^{th} particle by the fluid is counter-balanced by the contact forces exerted by the particles in contact with that particle. The particles are assumed to be strictly rigid and frictionless, so the contact forces between the particles are purely repulsive. We denote the contact forces between the k^{th} and i^{th} particles by f_{ik} ; here and in the following we will conventionally set repulsive forces to be positive, i.e. $f_{ik} \geq 0$. The force-balance condition then reads

$$-\vec{F}_k = \sum_{i \text{ in contact with } k} f_{ik} \vec{n}_{ik} , \quad (2)$$

where \vec{n}_{ik} is a unit vector pointing from the center of the i^{th} particle to the center of the k^{th} particle.

In Fig. 1 both results described above are illustrated, see figure caption for details.

3. Equation of motion

From relations (i) and (ii) in the previous section we now derive the exact equation of motion. Consider a system of N hard spheres (referred to in the following as particles) in a volume V in

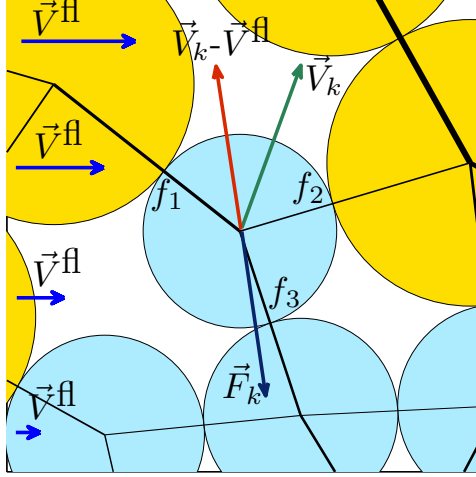


Figure 1: Illustration of the two main relations defining the model. Rigid particles are immersed in a viscous fluid described by the velocity field \vec{V}^{fl} (horizontal arrows on the left). The k^{th} particle in the center is moving with the velocity \vec{V}_k , and the difference between the k^{th} particle's velocity and the velocity of the underlying fluid is $\vec{V}_k - \vec{V}^{\text{fl}}$. The drag force on the k^{th} particle, \vec{F}_k , is proportional and opposite in sign to $\vec{V}_k - \vec{V}^{\text{fl}}$. Finally, the overdamped dynamics imply that the drag force \vec{F}_k is balanced by the vector-sum of the contact forces f_1, f_2 and f_3 .

d dimensions, such that there are no overlapping particles, and some of the particles are exactly in contact: the distance between their centers is equal to the sum of their radii. When the system is unjammed, the number of contacts N_c in the system remains smaller than the number of spatial degrees of freedom $Nd - d$. Note that we subtract d translations but not rotations due to the periodic boundary conditions. We denote the d dimensional vector of the i^{th} particle coordinates as \vec{R}_i , its time derivative as \vec{V}_i , and define the directional differences $\vec{R}_{ij} = \vec{R}_j - \vec{R}_i$, the pairwise distances $r_{ij} = \sqrt{\vec{R}_{ij} \cdot \vec{R}_{ij}}$, and the normalized directions $\vec{n}_{ij} = \vec{R}_{ij}/r_{ij}$. We will refer to the *contact network* as the set of all pairs of particles that are in contact at some instance in time, and the geometric information that accompanies the network, namely the directions \vec{n}_{ij} , and the pairwise distances r_{ij} .

The rate of change induced to a pairwise distance r_{ij} , given some vector of particles' velocities \vec{V}_k , follows:

$$\dot{r}_{ij} = \sum_k \frac{\partial r_{ij}}{\partial \vec{R}_k} \cdot \vec{V}_k = \sum_k (\delta_{jk} - \delta_{ik}) \vec{n}_{ij} \cdot \vec{V}_k = (\vec{V}_j - \vec{V}_i) \cdot \vec{n}_{ij} . \quad (3)$$

Fig. (2) illustrates how the velocities \vec{V}_k translate to the rate of change of pairwise distances r_{ij} . The above relation consists of a linear transformation of vectors from *the space of the particles* (of

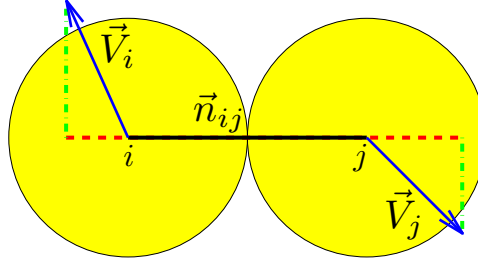


Figure 2: Given the velocities of the particles \vec{V}_k , the rate of change in the pairwise distance r_{ij} is the projection of the velocities on the direction \vec{n}_{ij} , see Eq. (3).

dimension Nd) to vectors in *the space of contacts* (of dimension N_c). We define

$$\mathcal{S} \equiv \frac{\partial r_{ij}}{\partial \vec{R}_k} , \quad (4)$$

then Eq. (3) can be written in bra-ket notation as

$$|\dot{r}\rangle = \mathcal{S}|V\rangle . \quad (5)$$

Here and in the following we denote vectors from the space of the particles with upper-case notation (e.g. $|V\rangle$ for particle velocities), and vectors from the space of contacts with lower-case notation (e.g. $|r\rangle$ for the vector of pairwise distances).

As the particles are completely rigid, they cannot penetrate each other. In addition, a given set of contacts does not change except at discrete points in time (see discussion in Sect. 4). Except for at those discrete time points, the velocities must satisfy

$$|\dot{r}\rangle = \mathcal{S}|V\rangle = 0 . \quad (6)$$

We define the *nonaffine velocities* as the difference between the total velocities of the particles and the affine velocity of the underlying fluid:

$$|V^{\text{na}}\rangle \equiv |V\rangle - |V^{\text{fl}}\rangle . \quad (7)$$

Combining with Eq. (6), the condition of no overlaps becomes

$$\mathcal{S}|V\rangle = \mathcal{S}(|V^{\text{fl}}\rangle + |V^{\text{na}}\rangle) = 0 , \quad (8)$$

or

$$\mathcal{S}|V^{\text{na}}\rangle = -\mathcal{S}|V^{\text{fl}}\rangle . \quad (9)$$

Since $|V^{\text{fl}}\rangle$ is perscribed by the model, the right-hand-side (RHS) of the above equation is known. However, it cannot be solved for $|V^{\text{na}}\rangle$, as \mathcal{S} is generally not square, and hence cannot be inverted. This is because the number of contacts N_c (the number of linear equations in Eq. (9) to be solved), is smaller than the number of degrees of freedom $Nd - d$ (the number of variables in Eq. (9)).

We now use the relations in Eq. (1) and Eq. (2). We first recall that the drag forces $|F\rangle$ exerted on the particles by the fluid are proportional and opposite in sign to the difference between the particles' velocities $|V\rangle$ and the affine velocity of the fluid $|V^{\text{fl}}\rangle$. Thus the drag forces are proportional and opposite in sign to the nonaffine velocities defined in Eq. (7), namely

$$-|F\rangle = \eta_0 (|V\rangle - |V^{\text{fl}}\rangle) = \eta_0 |V^{\text{na}}\rangle , \quad (10)$$

which is the same equation as Eq. (1), but in bra-ket notation. Without loss of generality we choose η_0 as our unit of viscosity; the above relation is thus

$$-|F\rangle = |V^{\text{na}}\rangle . \quad (11)$$

Due to the overdamped nature of our model the drag forces exerted on the particles by the fluid are exactly balanced by the contact forces between the particles. Starting from Eq. (2), we have

$$-\vec{F}_k = \sum_{i \text{ in contact with } k} f_{ik} \vec{n}_{ik} = \sum_{\text{all contacts } i,j} f_{ij} (\delta_{jk} - \delta_{ik}) \vec{n}_{ij} = \sum_{\text{all contacts } i,j} f_{ij} \frac{\partial r_{ij}}{\partial \vec{R}_k} . \quad (12)$$

The above relation consists of a linear transformation from contact-space to particle-space; the transformation is identical to the one defined in Eq. (4), namely $\frac{\partial r_{ij}}{\partial \vec{R}_k}$. However, it operates on a vector in contact space, as opposed to Eq. (3) where the transformation operates on a vector in particle-space. Thus, Eq. (12) becomes [17, 18]:

$$-|F\rangle = \mathcal{S}^T |f\rangle , \quad (13)$$

where $|f\rangle$ is the vector of contact forces. Combining Eq. (11) and Eq. (13), we obtain the relation between the nonaffine velocities and contact forces:

$$|V^{\text{na}}\rangle = \mathcal{S}^T |f\rangle . \quad (14)$$

Inserting the above relation in Eq. (9)

$$\mathcal{S}|V^{\text{na}}\rangle = \mathcal{S}\mathcal{S}^T|f\rangle = \mathcal{N}|f\rangle = -\mathcal{S}|V^{\text{fl}}\rangle , \quad (15)$$

where we have introduced the \mathcal{N} -matrix, defined as

$$\mathcal{N} \equiv \mathcal{S}\mathcal{S}^T . \quad (16)$$

By definition the \mathcal{N} -matrix is a symmetric semi-positive definite matrix, hence unless it is singular (see Subsect. 5.3 for discussion), Eq. (15) can be inverted in terms of the contact forces $|f\rangle$ as

$$|f\rangle = -\mathcal{N}^{-1}\mathcal{S}|V^{\text{fl}}\rangle . \quad (17)$$

As mentioned above, the velocity field of the fluid is perscribed by the model, therefore the above relation completely determines the contact forces. Now, using Eq. (14) the nonaffine velocities are obtained as

$$|V^{\text{na}}\rangle = \mathcal{S}^T|f\rangle = -\mathcal{S}^T\mathcal{N}^{-1}\mathcal{S}|V^{\text{fl}}\rangle . \quad (18)$$

This completes the derivation of our equations of motion; the velocities consist of affine and nonaffine contributions:

$$|V\rangle = |V^{\text{fl}}\rangle + |V^{\text{na}}\rangle , \quad (19)$$

where the affine term $|V^{\text{fl}}\rangle$ is perscribed by the model, and the nonaffine part $|V^{\text{na}}\rangle$ is determined by Eq. (18).

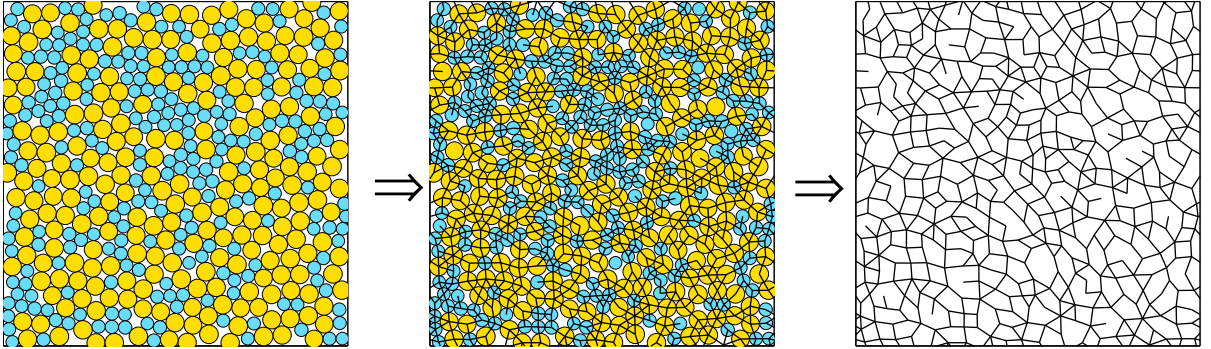


Figure 3: The instantaneous contact network is defined at any instance in time by collecting the set of all pairs of particles in contact, and extracting the geometric information of the corresponding network.

4. Instantaneous contact network

The equations of motion derived above hold for a single instance in time. They are entirely based on the geometric information encoded in the operator \mathcal{S} , which is defined on the existing set of contacts at that time. Given a configuration of the system we consider all the pair of particles in contact as our contact network (see Fig. 3), and based on this set we calculate the operator \mathcal{S} . However, this set of contacts is ever-changing, as particles move apart or collide. Nevertheless, the events of ‘breaking’ a contact between two particles, or the formation of a new contact between two colliding particles, are instantaneous. As a result, one can define time intervals in which a specific contact network remains intact. These time intervals are exactly the periods between any such event of contact-breaking or contact-formation, as illustrated in Fig. 4.

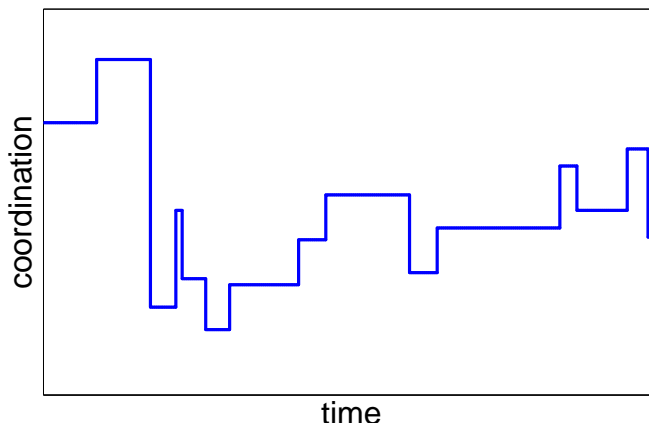


Figure 4: A typical signal of the instantaneous average coordination evolving in time. A contact network remains intact during the time intervals between events of contact formation/breaking.

The idea of an instantaneous contact network is central to our simulation method. In the subsequent explanations of the simulation method, we will often refer to the contact network, and to the consequence of adding or removing pairs of particles from it.

5. Simulational scheme

We now describe our simulation scheme. The main idea is to evolve the system by integrating Eq. (19) in time increments δt , until an occurrence of an event in which the contact network changes. These instances are inferred by considering the following three conditions at all times:

- (a) The distance between the centers of particles that are in contact is (up to integration errors to be discussed in the following) the sum of their radii.

- (b) Particles that are not in contact do not overlap.
- (c) The contact forces $|f\rangle$ (given by Eq. (17)) between particles in contact are positive.

The main simulation scheme is as follows:

- (i) Given a contact network at some instance t in which all contact forces are positive, an integration step δt , and the particles' velocities $|V\rangle$, calculate the time t_{col} at which the next collision will occur. The calculation of the next collision time is identical to the well-known calculation of the next collision time in event-driven hard sphere simulations, see for example [19]. However, the set of pairs of particles considered for a possible future collision are only those which are not already in contact.
- (ii) Compare t_{col} with $t + \delta t$; then
 - (ii.a) If $t_{\text{col}} < t + \delta t$, integrate Eq. (19) up to t_{col} , and add the colliding pair of particles to the contact network. This addition may render some of the other contact forces of the network negative. If indeed the collision results in negative contact forces, they are removed at this point by the procedure described in Subsect. 5.1.
 - (ii.b) If $t_{\text{col}} > t + \delta t$, integrate Eq. (19) up to $t + \delta t$, calculate the contact forces at the new state via Eq. (17), and check whether any of the contact forces has become negative. Remove the contacts with negative forces from the contact network.
- (iii) Step (ii) produces an updated contact network with strictly positive contact forces and no overlapping particles. The new velocities $|V\rangle$ are then calculated via Eqs. (18) and (19). Goto (i).

The integration step δt in our simulations is set by requiring that the number of integration steps between events (new contact formations or vanishing contact forces) is on average larger than 10. Satisfying this criterion requires gradually smaller integration steps for larger or denser systems. Moreover, in our simulations we bound the integration step by requiring $\delta t < 10^{-5}$.

In the following subsections we will explain how contact forces, which are rendered negative by the formation of a new contact, are filtered out of the contact network, and estimate the errors of the simulation.

5.1. Filtering out contacts with negative forces from the contact network

As mentioned above, the creation of a new contact may lead to breaking of existing contacts. The determination of the new contact network after detection of negative contact forces is carried out by repeating two procedures:

- (i) First, we successively remove the contact with the most negative force from the contact network, and re-calculate the contact forces via Eq. (17) after each such removal. The identity of all the contacts removed from the contact network during this procedure is stored. This removal procedure is carried out iteratively until the contact network is free of negative forces. Then, the total velocities are calculated using Eqs. (18) and (19).
- (ii) With the velocities $|V\rangle$ calculated at the end of procedure (i), we now consider the list of *removed contacts* that we have constructed during procedure (i). For each removed contact, we calculate the pairwise velocity

$$v_{ij} \equiv \dot{r}_{ij} = \vec{n}_{ij} \cdot (\vec{V}_j - \vec{V}_i) , \quad (20)$$

where the pair (i, j) no longer belongs to the contact network. Note that since we are considering pairs of particles which are no longer in contact, constraint (6) does not apply, and generally $v_{ij} \neq 0$. For some of the pairs considered one may find that $v_{ij} < 0$ which means that the particles (i, j) which were a part of the contact network are now *approaching* each other after breaking the contact between them. This scenario violates the no-overlapping condition, since this pair is (ideally) just in contact (it was just removed from the contact network), hence if this pair has $v_{ij} < 0$, it will instantly create an overlap. We treat this scenario explicitly – the pair with the most negative v_{ij} is then re-connected and added back to the contact network, and the contact forces are then re-calculated. If there remain any negative contact forces ($f_{ij} < 0$), or if pairs of particles *that were removed* from the contact network are still approaching each other ($v_{ij} < 0$), return to (i). Otherwise, the final contact network has been found. The uniqueness of the contact network obtained using the above procedure is demonstrated in the Appendix A.

5.2. Maintaining correctness and error estimations

The integration errors in distances between pairs of particles that belong to the instantaneous contact network are of order δt^2 . This can be shown by returning to Eq. (6), and writing it for a pair i, j as

$$v_{ij} = \dot{r}_{ij} = (\vec{V}_j - \vec{V}_i) \cdot \vec{n}_{ij} = 0 , \quad (21)$$

thus the velocity differences are orthogonal to the unit vectors \vec{n}_{ij} of pairs of particles in contact, see Fig. 5. Although the errors in the pairwise distances are very small, they can accumulate over many integration steps. To prevent the accumulation of large errors in cases where the lifetime of contacts is long, we utilize the following correction procedure periodically:

- (i) For each pair i, j in the contact network, calculate the pairwise errors $\delta r_{ij} = r_{ij} - (d_i + d_j)$, where d_i is the radius of the i^{th} particle.

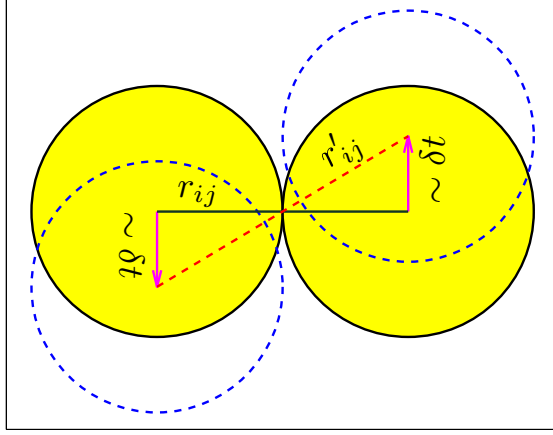


Figure 5: The continuous (dashed) particles are depicted before (after) a displacement of order δt . The change in the distance between two particles in contact is of order $r'_{ij} - r_{ij} \sim \delta t^2$ due to the orthogonality of the total velocity differences with respect to the unit vector \vec{n}_{ij} , see Eq. (21).

(ii) Denoting the pairwise errors as $|\delta r\rangle$, we calculate the correction displacement field

$$|\delta R\rangle = -\mathcal{SN}|\delta r\rangle. \quad (22)$$

(iii) At this stage the displacement field $|\delta R\rangle$ is treated as a velocity field; we then evolve the system in the direction determined by $|\delta R\rangle$, either until the entire displacement is achieved, or up to a collision induced by the evolution. Given displacements $|\delta R\rangle$ we calculate the next ballistic collision time t_{col} of pairs of particles that do not belong to the contact network, and record their identities.

(iii.a) If $t_{\text{col}} < 1$, update the coordinates via $|R\rangle \leftarrow |R\rangle + t_{\text{col}}|\delta R\rangle$, and add the colliding pair of particles to the contact network.

(iii.b) If $t_{\text{col}} > 1$, update the coordinates via $|R\rangle \leftarrow |R\rangle + |\delta R\rangle$.

(iv) If a new contact was formed in step (iii), repeat steps (i) – (iii) until no new contacts are formed.

(v) Calculate the contact forces, and filter out negative contact forces using the procedure described in Subsect. 5.1.

This correction procedure eliminates the accumulated errors in the pairwise distance between particles which are part of the contact network; the correction displacements $|\delta R\rangle$ can be thought of as the response of the system to an inhomogeneous expansion of the pairwise distances of the contacts within the contact network. The frequency of application of the correction procedure can be tuned to achieve the desired accuracy of the pairwise distances within the contact network.

5.3. Generating jammed configurations

Our simulation can be used to generate jammed configurations, under shear deformation or under compression (or both). Before explaining how such configurations can be generated, we first clarify the distinction between jammed and potentially jammed configurations.

In a *potentially jammed* configuration the ratio between the number of contacts and the number of degrees of freedom is such that the matrix \mathcal{S} must have a kernel of dimension one. Thus there exists a non-trivial vector of contact forces $|f_0\rangle \neq 0$ that satisfies force balance, i.e. that solves the equation $\mathcal{S}^T|f_0\rangle = 0$. However, a potentially jammed configuration may not be jammed, since the vector $|f_0\rangle$ that solves $\mathcal{S}^T|f_0\rangle = 0$ may have negative components, which cannot represent contact forces between rigid, frictionless particles. Therefore, in a *jammed* configuration there must exist a vector of positive contact forces $|f_0\rangle > 0$, that solves the equation $\mathcal{S}^T|f_0\rangle = 0$.

In order to generate such jammed configurations, one must handle the problematic cases in which the system becomes potentially jammed. In these cases, the equation $\mathcal{S}^T|f\rangle = 0$ has a non-trivial solution, which means that $\mathcal{N} \equiv \mathcal{S}\mathcal{S}^T$ has a zero eigenvalue, which in turn implies that Eq. (17) cannot be solved, thus the contact forces and the velocities cannot be calculated.

The detection of potentially jammed or jammed configurations requires the tracking of the coordination number of the *constrained subset* of the system. The constrained subset is the set of particles which are in contact with at least $d + 1$ other particles from the constrained subset (where d is the spatial dimensionality of the system considered). The calculation of the constrained subset must be performed iteratively, since the removal of some of the particles from the constrained subset may exclude other particles connected to them from the constrained subset as well. From a physical perspective, the monitoring of the constrained subset eliminates the problems of counting degrees of freedom associated with rattlers or particles which are just loosely connected in the contact network.

With the correct detection of the constrained subset in hand, we next define the constrained coordination number \bar{z} as

$$\bar{z} \equiv \frac{1}{\bar{N}} \left(2(d-1) + \sum_{i \in \text{constrained subset}} \bar{z}_i \right), \quad (23)$$

where \bar{z}_i is the number of contacts between the i^{th} particle and other particles j which have $\bar{z}_j \geq d+1$, and \bar{N} is the number of particles i with $\bar{z}_i \geq d+1$. The system is potentially jammed if $\bar{z} = 2d$. Eq. (23) is obtained by comparing the number of contacts in the constrained subset $\frac{1}{2} \sum_i \bar{z}_i$ to the

number of degrees of freedom $\bar{N}d - d + 1$. The addition of one to the number of degrees of freedom assures that \mathcal{S} has a kernel of dimension one if the system is potentially jammed. Definition (23) should be calculated using integer arithmetics, since it is an exact indicator of isostaticity¹.

Once a potentially jammed configuration has been detected, the vector $|f_0\rangle$ which solves $\mathcal{S}^T|f_0\rangle = 0$ is calculated [20]. If all its components are positive, the system is jammed. Otherwise, the procedure described in Subsect. 5.1 for filtering negative contact forces out of the contact network is employed, assigning the solution $|f_0\rangle$ as the contact forces. Within the procedure, the constrained coordination number must always be tracked; whenever the system is detected to be potentially jammed, the solution $|f_0\rangle$ should be re-calculated and considered instead of the contact forces. The procedure ends with either (i) some contacts being removed such that the system is no longer potentially jammed, then the forces and velocities can be calculated as usual, or (ii) a contact network being formed with a solution $|f_0\rangle$ to $\mathcal{S}^T|f_0\rangle = 0$, having only positive components, then a jammed configuration has been found.

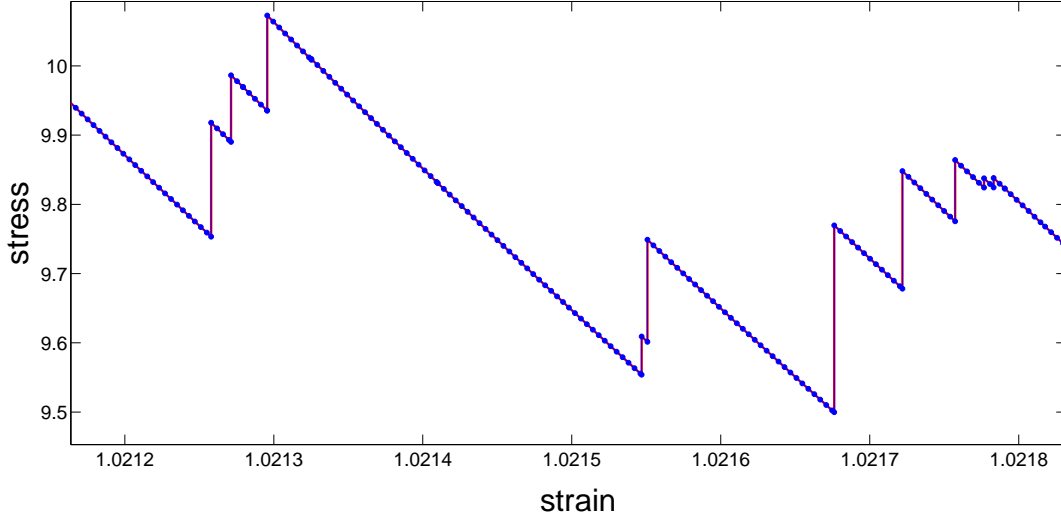


Figure 6: Segment of a typical stress vs. strain signal from our event-driven simulation, at volume fraction of $\phi = 0.83$. The stress relaxes during the time intervals in which the contact network remains intact. The sudden upward jumps in stress signal the collision of particles. Our simulation method enables an accurate study of the statistics of the collisions and their effect on the mechanical response of the system.

¹This indicator is exact if there are no over-constraints regions in the sample. This is the case for polydisperse particles where crystalline over-coordinated regions cannot appear.

6. Results

We simulate systems of discs in two dimensions, under simple shear flow. Our system consists of a binary mixture, where half of the discs are small and half are large. We add a uniform polydispersity of 3% to avoid hexagonal patches of identical particles². Our unit of length λ is the mean diameter of the small particles. The large particles have a mean radius of 0.7λ and the small particles have a mean radius of 0.5λ . The velocity field of the underlying fluid is $\vec{V}^{\text{fl}}(\vec{R}) = y\hat{x}$. Simple shear flow is imposed homogeneously through the simulation cell using Lees-Edwards boundary conditions [19]. Detection of newly formed contacts is achieved by maintaining data structures of neighbor-lists which are updated using cell-subdivisions that allow for the calculation of the neighbor-lists in a time which is linear in the system size [19]. The equation of motion (19) is integrated by solving Eq. (17) using a standard conjugate gradient algorithm [21].

In Fig. (6) we plot a small segment of a typical stress vs. strain signal from our simulations at a volume fraction of $\phi = 0.83$. The stress σ is measured using information of the contact forces via

$$\sigma = -\frac{\langle f|\mathcal{S}|V^{\text{fl}}\rangle}{\mathcal{V}} , \quad (24)$$

where \mathcal{V} is the volume of the system. The signal displays a series of intervals in which the stress relaxes, interrupted by abrupt increases in the stress, which are the consequence of collisions (new contacts are formed).

In Fig. (7) we display a realization of our sheared systems at $\phi = 0.83$. The thickness of the lines connecting the centers of neighboring particles are proportional to the contact force between the particles.

6.1. Comparison with steepest descent simulations

An alternative to integrating our equation of motion, Eq. (19), one can apply small strain-steps followed by the minimization of a soft, repulsive interaction potential by means of steepest descent, i.e. according to the first order equation of motion

$$\dot{\vec{R}}_k = -\eta_0 \nabla_k U , \quad (25)$$

where a possible choice of the potential energy is $U = \sum_{i,j>i} \phi(r_{ij})$, and

$$\phi(r_{ij}) = \begin{cases} \varepsilon \left(1 - \frac{r_{ij}}{d_i + d_j}\right)^2 & , \quad r_{ij} < d_i + d_j \\ 0 & , \quad r_{ij} > d_i + d_j \end{cases} , \quad (26)$$

²Such patches can be hyperstatic, i.e. over-constrained. Physically these patches move as solid blocks, until they break. In our approach these patches are difficult to deal with (although it can be done), as they lead to zero modes in the spectrum of \mathcal{N} , which renders Eq. (17) difficult to solve numerically. We avoid this problem by adding polydispersity.

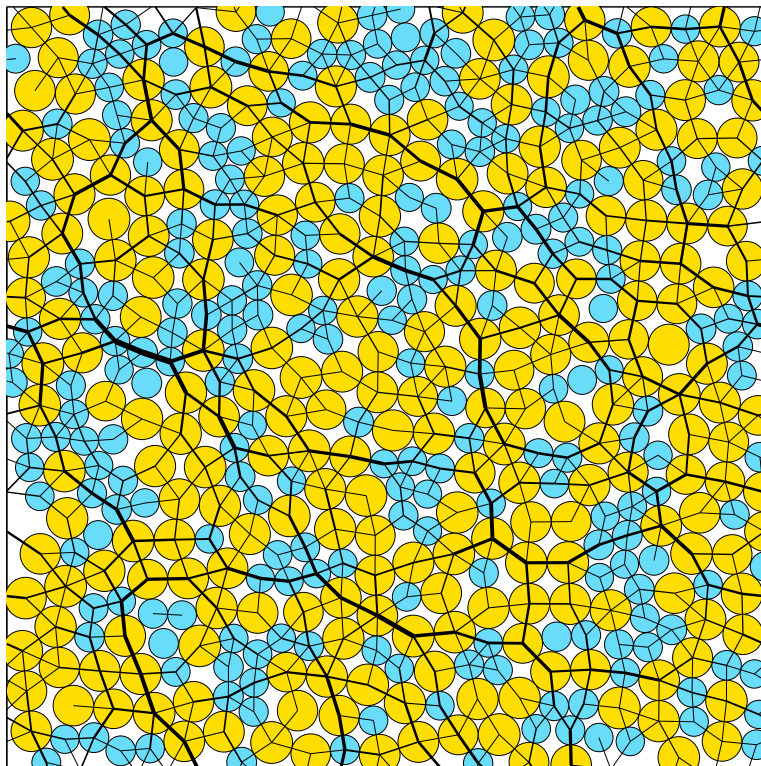


Figure 7: A snapshot from our two-dimensional simulations of bi-disperse discs under shear flow. The thickness of the lines connecting the centers of the particles represent the magnitude of the contact forces between the particles. The colors distinguish between the two sizes of discs.

where ε is an energy scale and d_i is the radius of the i^{th} particle. The equivalence between the two approaches stems from (i) the identical dissipation mechanism, which only acts along the nonaffine part of the motion, and (ii) the total evolution that keeps the potential energy at zero since the system is studied in the floppy regime, where it is always possible to re-arrange the particles to a state of zero potential energy. This is analogous in our simulation to the no-overlap condition which is always satisfied. To validate our simulational scheme, we compare the results of our scheme with the steepest descent (SD) simulations. In the SD simulation, we construct a tentative contact network by considering pairs of particles that satisfy $r_{ij} = d_i + d_j + \delta r$ with $\delta r = 10^{-5}$. This network is constructed only for the contact force calculation from which the stress is deduced. We choose the strain increment for the SD simulations to be $\delta\gamma = 10^{-6}$ and choose the stopping condition for the minimization to be $\max(\nabla_i U) < 10^{-9}\varepsilon/\lambda$. The integration step for the steepest descent minimizations was set to be $\delta t = 0.1$. In Fig. 8 we plot the trajectories of the stress vs. strain

for both simulation schemes, for systems of $N = 100$ particles at the volume fraction $\phi = 0.82$. The agreement between the two signals vindicates our event-driven scheme. We note that for strain increments of $\delta\gamma = 10^{-6}$, with which the events of contact formations can be clearly singled out in the SD simulations, the running time is extremely long, hence the choice of small systems for comparison with our method. It took over 30 hours on a conventional workstation to produce the data of Fig. 8 using the SD method, whereas it takes just a few minutes with our event driven code on the same machine.

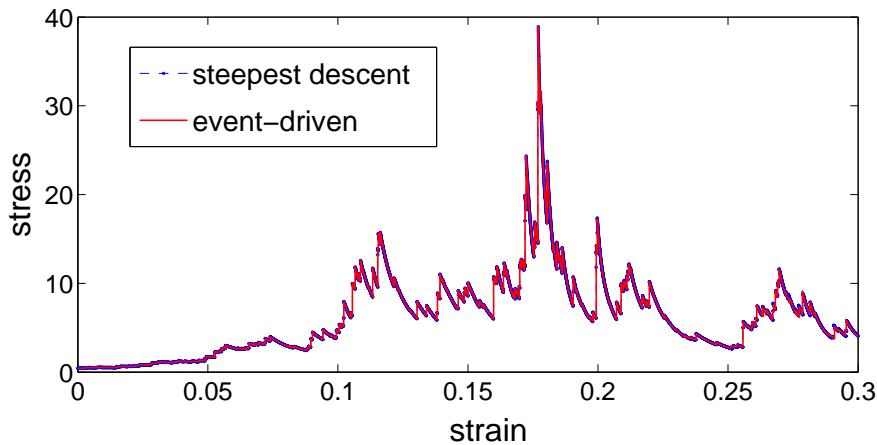


Figure 8: Comparison between stress vs. strain trajectories from our event-driven simulation and from the steepest descent method. Starting from the same initial configurations, the trajectories remain essentially identical for tens of percents of strain, vindicating our event-driven scheme.

7. Discussion

We have introduced an event-driven simulation scheme for a simple model for dense suspension flow. The simulation is based on an equation of motion which is exactly derivable from the model assumptions. The simulation maintains the conditions of no overlaps and strictly positive contact forces between the rigid particles at all times. We have introduced a procedure that allows for the correction of the integration errors in the pairwise distances between particles that are part of the instantaneous contact network. We have also provided a prescription for generating jammed configurations employing our method, under compression or shear.

We have demonstrated that our method produces essentially identical results to steepest-descent minimization methods, though at greatly reduced computational cost as well as increased robustness and accuracy of the contact network information. Indeed, the main virtue of our event-driven method

is the control over the identity of the contact network that allows for careful study of the statistics of contact formation and breakage. In our approach there are no uncertainties nor arbitrary thresholding associated with the definition of which particles should be considered as contacts. This advantage becomes increasingly important closer to jamming where contacts rearrange very rapidly, and where many particles are very close but actually not in contact.

Acknowledgements

We thank Yael Elmatad for her comments. This work has been supported by the Sloan Fellowship, NSF DMR-1105387 (2011), and Petroleum Research Fund #52031-DNI9.

Appendix A. Uniqueness of the contact network upon new contact formation

The algorithm described in Subsect. 5.1 begins with the full set of contacts, including a newly formed contact. We denote this full set of contacts by Ω . Upon termination, the algorithm produces a subset of contacts, denoted here by A , which satisfies the two following conditions:

- (i) all of the contact forces calculated on the subset A of contacts are positive, and
- (ii) all of the pairs of particles which were *just removed* from the contact network, are moving away from each other.

In this subsection we prove that the contact network found by our algorithm is unique. We first re-iterate that the operators \mathcal{S} and \mathcal{N} (Eqs. (4) and (16) respectively) are generally defined on a given set of contacts. When a new contact is formed, the set of pairs on which these operators are defined grows by one pair – the new contact. However, as mentioned above, the formation of a new contact may render other contact forces negative, in which case those pairs with negative contact forces are removed from the contact network. Removing contacts from the contact network re-defines the operators \mathcal{S} and \mathcal{N} , since the space of contacts has changed. Given the subset of contacts $A \subseteq \Omega$, we denote the corresponding operators defined on this set as \mathcal{S}_A and \mathcal{N}_A . As opposed to the space of contacts, the space of particles never changes; one can, in principle, calculate the full vector of velocities given any subset of the full contact space. For instance, the velocities calculated using the subset A are

$$|V_A\rangle = |V^{\text{fl}}\rangle + |V_A^{\text{na}}\rangle = |V^{\text{fl}}\rangle - \mathcal{S}_A^T \mathcal{N}_A^{-1} \mathcal{S}_A |V^{\text{fl}}\rangle . \quad (\text{A.1})$$

We now present the general relation between contact forces and velocities; starting from Eq. (14), we consider the full contact network, then

$$\mathcal{S}^T |f\rangle = |V^{\text{na}}\rangle = |V\rangle - |V^{\text{fl}}\rangle . \quad (\text{A.2})$$

Operating with \mathcal{S} on both sides of the above equation,

$$\mathcal{S}\mathcal{S}^T|f\rangle = \mathcal{N}|f\rangle = \mathcal{S}|V\rangle - \mathcal{S}|V^{\text{fl}}\rangle . \quad (\text{A.3})$$

Now, inverting to solve for the contact forces

$$|f\rangle = \mathcal{N}^{-1}\mathcal{S}|V\rangle - \mathcal{N}^{-1}\mathcal{S}|V^{\text{fl}}\rangle . \quad (\text{A.4})$$

Given any velocity vector $|V\rangle$, the resulting contact forces can be obtained via Eq. (A.4). This equation is more general than Eq. (17), which is obtain from the above relation by demanding that $\mathcal{S}|V\rangle = 0$, which is the condition for maintaining an intact contact network. In our discussion we relax this condition for a subset of the contact network, since removing contacts will result in non-zero pairwise velocities.

We next note that a contact force which is identically zero has no effect on the dynamics. This can be understood by re-examining Eq. (14); a zero contact force does not participate in the vector sum of the contact forces on each particle, which, in turn, is equal to the nonaffine velocities. This allows us to carry out the entire discussion in the full space of contacts Ω ; the vector of contact forces in the full space of contacts, obtained with the velocities calculated on the subset A , is

$$|f_A\rangle = \mathcal{N}^{-1}\mathcal{S}|V_A\rangle - \mathcal{N}^{-1}\mathcal{S}|V^{\text{fl}}\rangle \quad (\text{A.5})$$

Note that the dimension of $|f_A\rangle$ is the size of the full set of contacts $|\Omega|$. Labeling contact components by $\alpha \in \Omega$, and denoting by $|\delta_\alpha\rangle$ a vector which is unity in the α component and zero otherwise, the condition of positive contact forces now reads

$$\begin{aligned} \langle \delta_\alpha | f_A \rangle &> 0 \quad \text{if} \quad \alpha \in A , \\ \langle \delta_\alpha | f_A \rangle &= 0 \quad \text{if} \quad \alpha \in \Omega \setminus A . \end{aligned} \quad (\text{A.6})$$

The vector of pairwise velocities induced by the particles' velocities $|V_A\rangle$ Eq. (A.1) is

$$|v_A\rangle = \mathcal{S}|V_A\rangle . \quad (\text{A.7})$$

The condition according to which pairs of particles that were just removed from the contact network should be moving apart can be written in our framework as

$$\begin{aligned} \langle \delta_\alpha | v_A \rangle &= 0 \quad \text{if} \quad \alpha \in A , \\ \langle \delta_\alpha | v_A \rangle &> 0 \quad \text{if} \quad \alpha \in \Omega \setminus A . \end{aligned} \quad (\text{A.8})$$

We now assume that there exists another different subset $B \subseteq \Omega, B \neq A$, and an associated velocity vector $|V_B\rangle = |V^{\text{fl}}\rangle - \mathcal{S}_B^T \mathcal{N}_B^{-1} \mathcal{S}_B |V^{\text{fl}}\rangle$, the contact forces $|f_B\rangle$ and the pairwise velocities $|v_B\rangle$, which also satisfy (A.6) and (A.8) for the subset B . We consider the contraction

$$\langle v_A - v_B | \mathcal{N}^{-1} | v_A - v_B \rangle > 0 , \quad (\text{A.9})$$

which is positive since \mathcal{N} is positive definite. Combining $|v\rangle = \mathcal{S}|V\rangle$ with Eq. (A.4) we have

$$|f_A - f_B\rangle = \mathcal{N}^{-1}\mathcal{S}|V_A\rangle - \mathcal{N}^{-1}\mathcal{S}|V_B\rangle = \mathcal{N}^{-1}|v_A - v_B\rangle . \quad (\text{A.10})$$

Inserting this back into Eq. (A.9), we find

$$\langle v_A - v_B | \mathcal{N}^{-1} | v_A - v_B \rangle = \langle v_A - v_B | f_A - f_B \rangle = \langle v_A | f_A \rangle + \langle v_B | f_B \rangle - \langle v_A | f_B \rangle - \langle v_B | f_A \rangle . \quad (\text{A.11})$$

From the conditions in Eq. (A.6) and Eq. (A.8), both $\langle v_A | f_A \rangle = 0$ and $\langle v_B | f_B \rangle = 0$. The inequality (A.9) now reads

$$0 < \langle v_A - v_B | \mathcal{N}^{-1} | v_A - v_B \rangle = -\langle v_A | f_B \rangle - \langle v_B | f_A \rangle < 0 , \quad (\text{A.12})$$

which is a contradiction, since the cross terms $\langle v_A | f_B \rangle > 0$ and $\langle v_B | f_A \rangle > 0$, as all components of v_A, v_B, f_A, f_B are non-negative by construction. Hence, there cannot exist another distinct subset $B \neq A$ which satisfies Eqs. (A.6) and (A.8), and therefore the subset A is unique.

References

- [1] A. Einstein, Ann. Physik. **19**, 289 (1906).
- [2] P. Chaudhuri, L. Berthier, and S. Sastry, Phys. Rev. Lett. **104**, 165701 (2010).
- [3] D. Vagberg, P. Olsson, S. Teitel, Phys. Rev. E **83**, 031307 (2011).
- [4] J. J. Stickel and R. L. Powell, Annu. Rev. Fluid Mech. **37** 129 (2005).
- [5] G. Ovarlez, F. Bertrand, and S. Rodts, J. Rheol. **50**, 259 (2006).
- [6] H. A. Barnes, M. F. Edwards, L. V. Woodcock, Chem. Eng. Sci. 42(4):591 (1987).
- [7] P. Olsson and S. Teitel, Phys. Rev. Lett. **99**, 178001 (2007).
- [8] P. Olsson and S. Teitel, Phys. Rev. E **83**, 030302(R) (2011).
- [9] D. J. Durian, Phys. Rev. Lett. **75**, 4780 (1995).
- [10] D. J. Durian, Phys. Rev. E **55**, 1739 (1997).
- [11] D. Vagberg, D. V.-Balderas, M. A. foore, P. Olsson, and S. Teitel, Phys. Rev. E **83**, 030303(R) (2011).
- [12] C. Heussinger and J.-L. Barrat, Phys. Rev. Lett. **102**, 218303 (2009).

- [13] C. Heussinger, L. Berthier, and J.-L. Barrat, Europhys. Lett. **90**, 20005 (2010).
- [14] T. Hatano, J. Phys. Soc. Jpn. **77** 123002 (2008).
- [15] T. Hatano, Phys. Rev. E **79**, 050301(R) (2009).
- [16] F. Radjai and V. Richefeu, Mech. Mater. **41**, 715 (2009).
- [17] J. -N. Roux, Phys. Rev. E **61**, 6802 (2000).
- [18] M. Wyart, Annales de Physiques Fr., Chapter 7, **30**, 1, 2005
- [19] M. P. Allen and D. J. Tildesley, *Computer Simulations of Liquids* (Oxford Univ. Press, New York, 1991).
- [20] As $|f_0\rangle$ is the eigenvector associated with the zero eigenvalue of \mathcal{N} , it can be calculated via diagonalization, for instance.
- [21] W. H. Press, S. A. Teukolsky, W. T. Vetterling, and B. P. Flannery, *Numerical Recipes in C—The Art of Scientific Computing*, 2nd ed. (Cambridge Univ. Press, Cambridge, 1994).